

Dancing bubble sonoluminescence in phosphoric acid solution

Dexin Wang(王德鑫), Qinghim(清河美), Wurihan Bao(包乌日汗), Haiying Han(韩海英), and Naranmandula(那仁满都拉)

Citation: Chin. Phys. B, 2024, 33 (**11**): 117803. DOI: 10.1088/1674-1056/ad78dc
Journal homepage: http://cpb.iphy.ac.cn; http://iopscience.iop.org/cpb

What follows is a list of articles you may be interested in

Investigation of reflection anisotropy induced by micropipe defects on the surface of a 4H-SiC single crystal using scanning anisotropy microscopy

Wei Huang(黄威), Jinling Yu(俞金玲), Yu Liu(刘雨), Yan Peng(彭燕),Lijun Wang(王利军), Ping Liang(梁平), Tangsheng Chen(陈堂胜), Xiangang Xu(徐现刚), Fengqi Liu(刘峰奇), and Yonghai Chen(陈涌海)

Chin. Phys. B, 2024, 33 (**3**): 037801. DOI: 10.1088/1674-1056/acf27f

Elemental composition x-ray fluorescence analysis with a TES-based high-resolution x-ray spectrometer

Bingjun Wu(吴秉骏), Jingkai Xia(夏经铠), Shuo Zhang(张硕), Qiang Fu(傅强), Hui Zhang(章辉),Xiaoming Xie(谢晓明), and Zhi Liu(刘志)

Chin. Phys. B, 2023, 32 (**9**): 097801. DOI: 10.1088/1674-1056/acd926

Computational simulation of ionization processes in single-bubble and multi-bubble sonoluminescence

Jin-Fu Liang(梁金福), De-Feng Xiong(熊德凤), Yu An(安宇), and Wei-Zhong Chen(陈伟中)

Chin. Phys. B, 2022, 31 (**11**): 117802. DOI: 10.1088/1674-1056/ac6745

Computation and analysis of light emission in two-bubble sonoluminescence

Jin-Fu Liang(梁金福), Xue-You Wu(吴学由), Yu An(安宇), Wei-Zhong Chen(陈伟中), Jun Wang(王军)

Chin. Phys. B, 2020, 29 (**9**): 097801. DOI: 10.1088/1674-1056/ab969e

Abnormal ionization in sonoluminescence

Zhang Wen-Juan (张文娟), An Yu (安宇)

Chin. Phys. B, 2015, 24 (**4**): 047802. DOI: 10.1088/1674-1056/24/4/047802

Dancing bubble sonoluminescence in phosphoric acid solution

Dexin Wang(王德鑫)[1], Qinghim(清河美)[2], Wurihan Bao(包乌日汗)[1], Haiying Han(韩海英)[1], and Naranmandula(那仁满都拉)[1,†]

[1] *College of Physics and Electronics, Inner Mongolia Minzu University, Tongliao* 028043, *China*
[2] *Tongliao City No.* 4 *Middle School South Campus, Tongliao* 028000, *China*

(Received 14 June 2024; revised manuscript received 30 August 2024; accepted manuscript online 10 September 2024)

Sonoluminescence is more distinctly observed in phosphoric and sulfuric acid, which exhibit high viscosity and lower vapor pressures relative to water. Within an 85-wt% phosphoric acid solution saturated with argon (Ar), variations in the light-emitting regimes of bubbles were noted to correspond with increments in the driving acoustic intensity. Specifically, the bubbles were observed to perform a dance-like motion 2 cm below the multi-bubble sonoluminescence (MBSL) cluster, traversing a 25-mm^2 grid during the camera exposure period. Spectral analysis conducted at the beginning of the experiment showed a gradual attenuation of CN ($B^2\Sigma$–$X^2\Sigma$) emission concurrent with a strengthening of Ar (4p–4s) atom emission lines. The application of a theoretical temperature model to the spectral data revealed that the internal temperature of the bubbles escalates swiftly upon their implosion. This study is instrumental in advancing the comprehension of the underlying mechanisms of sonoluminescence and in the formulation of a dynamic model for the behavior of the bubbles.

Keywords: sonoluminescence, spectrum, phosphoric acid solution, noble gas

PACS: 78.60.Mq, 43.25.+y **DOI:** 10.1088/1674-1056/ad78dc

1. Introduction

Sonoluminescence (SL), the emission of light from liquids excited by ultrasonic waves, is a multifaceted phenomenon that has captivated researchers for decades due to its intriguing physical and chemical implications.[1,2] The interplay between acoustic cavitation, bubble dynamics, and light emission presents a rich area of study with potential applications in sonochemistry, material processing, and biomedical engineering.[3–5]

The study of SL is particularly enriched by the use of various liquid media as host fluids for experiments.[6–8] Concentrated solutions of sulfuric and phosphoric acid have been widely used to investigate SL, owing to their unique properties that favor stable bubble formation and enhanced light emission.[9–11] These solutions, with their high viscosity and low vapor pressure, facilitate more effective bubble collapse and provide a stable environment for the observation of both single bubble sonoluminescence (SBSL)[12–14] and multi-bubble sonoluminescence (MBSL).[15,16]

In the MBSL from concentrated sulfuric acid, emission lines characteristic of argon (Ar) atoms and sulfur monoxide (SO*) were observed.[17] This finding is mirrored in the SBSL spectrum, which emerged from concentrated sulfuric acid that had been degassed and subsequently saturated with Ar.[18] Notably, the detection of Ar atom emission lines in both cases challenges the different views previously proposed for MBSL and SBSL.[19]

Observations of luminescent jittering bubbles and fast-moving glowing bubbles in sulfuric and phosphoric acids under varying acoustic pressures have revealed new states of SL.[20,21] These states are mainly influenced by the acoustic pressures, the intrinsic properties of the liquid, and the interactions between the bubbles themselves. Consequently, the levitation of luminescent bubbles and their trajectories under different acoustic intensities have been a key point for research.

Furthermore, Xu *et al.* recorded the paths of moving-SBSL in 65-wt% phosphoric acid solution enriched with Ar using a digital camera.[22,23] It was observed that the dissolved rare gases led to an increase in both luminescence intensity and emission temperature. This phenomenon of moving-SBSL was initially observed by Suslick and colleagues in the year 2000 within N-methylformamide, distinguished by the characteristic non-stationary bubbles following circular or elliptical trajectories.[24] The modeling of moving-SBSL trajectories has incorporated the external pressure field and 'history' force, which plays a pivotal role in the unstable movement of bubbles.[25]

In the MBSL of 95-wt% sulfuric acid solution with 0.1-M Na_2SO_4, it was found that the light-emitting regimes of the bubble clusters transform from filamentous to bulbous and ultimately to cone-shaped with changes in acoustic intensity.[17,23] In these regimes, a distinct disparity in colors emerges between the top and bottom sections of the bubble cluster, indicating temperature inhomogeneity within the MBSL.[26,27]

†Corresponding author. E-mail: nrmdlbf@126.com

© 2024 Chinese Physical Society and IOP Publishing Ltd

In order to make a further insight into the SL phenomenon of acid solutions, we studied the MBSL within an 85-wt% phosphoric acid solution saturated with Ar. By adjusting the acoustic intensity, we captured the light-emitting regimes and bubble trajectories using high-speed imaging, while concurrently recording the SL spectrum at various intervals with a high-resolution spectrometer. The observed phenomena and spectral data were then simulated and analyzed using a motion and temperature model of the bubble located below the ultrasonic horn.

2. Experiment setup and result

The SL apparatus were used a 20-kHz UH-500A ultrasonic processing system. The experiments were performed in a cylindrical quartz cell with a diameter of 80 mm and a height of 150 mm, containing approximately 500 mL of an 85-wt% phosphoric acid solution saturated with Ar. The cell was open at the top, allowing for easy access and observation. The ultrasonic horn, with a tip diameter of 13 mm, was positioned 20 mm below the liquid surface. The SL spectrum were acquired using an SP-2-500i spectrometer equipped with a 300-grooves/mm grating blazed at 500 nm and a 1024 × 100 pixel liquid nitrogen-cooled CCD camera. To ensure minimal optical losses, an optical fiber directed emission from the luminescent bubbles to the spectrometer input slit, optimizing the accuracy of spectral data acquisition. A schematic diagram of the experimental configuration is provided in Fig. 1.

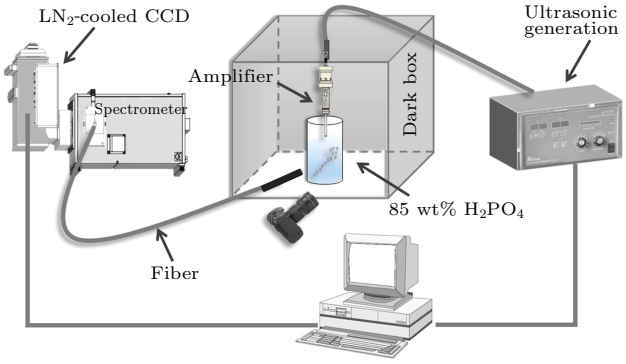


Fig. 1. Schematic diagram of the experimental setup.

Due to the high ambient solubility of atmospheric gases in 85-wt% phosphoric acid solution at room temperature and pressure, degassing and regassing procedures were necessary to control the Ar concentration. The solution is pretreated with vacuum and thermal degassing to remove dissolved gases, and then exposure to an Ar atmosphere over prolonged intervals to facilitate absorption. During these processes, the phosphoric acid solution was magnetically stirred within sealed vessels to accelerate the rate of gas evacuation and dissolution. Before the experiment commenced, the phosphoric acid solution was meticulously cooled to a precise temperature of 6.3 °C within a refrigeration unit. Subsequently, the solution was carefully decanted into a cylindrical quartz cell, designated for experimental procedures. It is noteworthy that the cuvette was not hermetically sealed, which led to a gradual increase in the gaseous content of the solution due to exposure to the ambient atmosphere throughout the duration of the testing phase.

2.1. The filaments structure of MBSL

The acoustic power of the ultrasonic generator was gradually increased during the experiments. At first, the number of light-emitting bubbles increased quickly as the acoustic power rose. Before the dissolved Ar significantly diffused away, filamentous formations were apparent around the horn at acoustic power of 22.6 W/cm^2 as shown in Fig. 2(a). Magnified subsets in Figs. 2(b)–2(d) show transient streamer formation and trajectories of discrete light-emitting bubble jets. This filamentous state was short-lived, transitioning to clustered bubbles as acoustic power continued to rise.

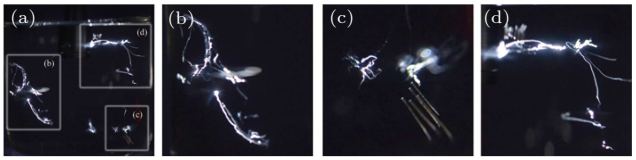


Fig. 2. The filamentous structures of light-emitting bubbles in phosphoric acid solution. Panels (b), (c), and (d) are enlarged portions of panel (a).

2.2. The dancing bubble SL

The increase in acoustic power of 30 W/cm^2 to the consolidation of the dancing bubbles SL into a relatively stable cluster. Concurrent high-speed optical imaging of the system illustrated complex trajectories of discrete bubbles approximately 2 cm from the cluster base. The tracking of these bubble trajectories was facilitated by continuous optical imaging using a camera with a 1/17-second exposure time. Figure 3 shows selected frames highlighting the interesting bubble dynamics observed during this high-power regime. The tracking of individual bubble trajectories can obtained information on the localized pressure and temperature conditions within the bubble cluster.

As shown in Fig. 3, a consolidated cluster of light-emitting bubbles stabilized 10 mm from the horn tip. Outside this cluster, a discrete bubble undergoing irregular trajectories is discernible. This dancing bubble has a significantly higher light output than the static cluster background when exposed to ambient lighting; it appears brighter to the camera as well as the unaided eye. As demonstrated in Figs. 4(a)–4(d), quantitative examination of several dancing bubbles displays linear

paths spanning 25 mm^2 across the camera exposure period before dissipating into the solution.

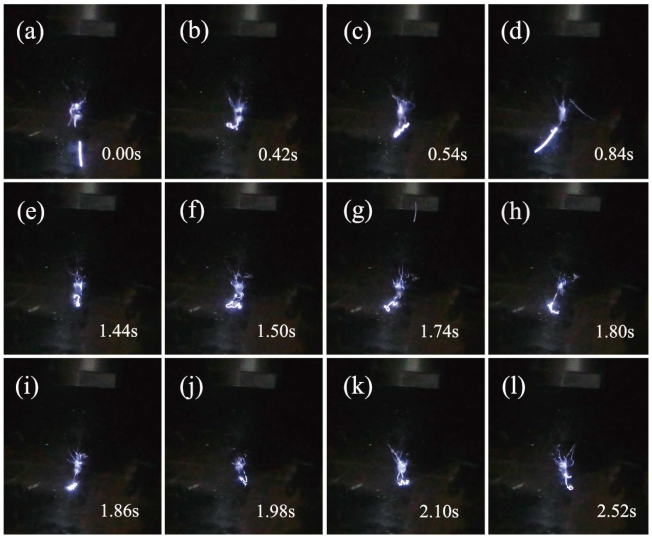


Fig. 3. The different trajectories of dancing bubble SL (under normal lighting conditions, 1/17 s exposure time). The tip of the probe (13 mm in diameter) is visible at the top of the picture.

The clustering and stabilization of the light-emitting bubbles can be attributed to the interplay of acoustic focusing, wall reflections, and Bjerknes forces within the cylindrical quartz cell. The ultrasonic horn situated along the central axis of the cell creates a focal zone that concentrates the cavitation activity and facilitates the attainment of the threshold value of SL intensity. A stable bubble cluster forms as a result of additional mediation of the bubble by the primary and secondary Bjerknes forces during acoustic excitation. Sometimes, dancing bubbles can be ejected from the cluster through inter-bubble collisions, freeing them from the secondary Bjerknes forces. These isolated bubbles then undergo more intense acoustic compression cycles, which can induce heightened interior temperatures and pressures, resulting in enhanced light emission. The observed dynamic behavior of dancing bubbles outside the stabilized cluster is likely a consequence of this mechanism, where the release from the secondary Bjerknes forces allows for more powerful bubble oscillations and collapse.

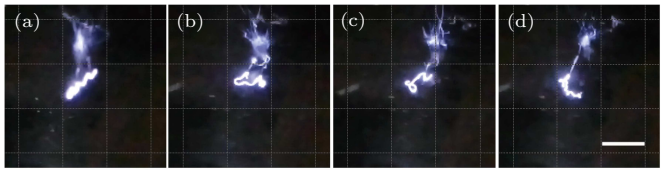


Fig. 4. The further enlargement of Figs. 3(c), 3(f), 3(g), and 3(h).

With continued increase in acoustic power, the dancing bubble SL disappeared, and the stabilized bubble cluster transitioned into an expanded cluster regime, which was consistent with previous observations in similar systems.[20]

The observed translation of dancing bubble SL is similar to previous described of moving-SBSL, commonly generated in flask-based systems.[20,28] Prospective trajectories under simple assumptions regarding the force balances on an isolated bubble have been investigated through simulation studies.[29,30] However, the irregular paths observed here significantly deviate from the predicted circular routes, suggesting that more complex dynamics and force components are dominant in this unknown region.

2.3. The SL spetrum

Spectroscopic quantification of the extreme temperatures and pressures generated during MBSL a primary experimental approach for study the underlying mechanisms. Smooth and intense emission spectrum of MBSL were acquired over 200 nm–900 nm for 85-wt% phosphoric acid solutions saturated with Ar.

The spectrum focuses on the range of 360 nm–630 nm when the dancing bubble SL first appears, with a peak at 380 nm that gradually becomes weaker over time, as shown in Fig. 5. Preliminary spectroscopic analyses evidenced a pronounced emission peak situated, which might be attributed to the CN ($B^2\Sigma$–$X^2\Sigma$) rovibronic transition. These spectrum signatures have been reported previously,[13] especially in cavitation experiments with moving-SBSL. The emergence of electronically excited-state CN radicals is indicative of the inception of sonochemical reactivity within the acoustically driven cavitation bubbles. Over extensive measurement durations, the signature CN emission line centered at 380 nm gradually disappeared. Meanwhile, a unique spectral line at 589 nm that is attributed to electrically excited-state Na^* appeared and intensified. The CN radicals and Na atom indicate continuous chemical evolution within the SL bubble. The initial advent of CN radicals suggests radical formation resulting from molecular decomposition and recombination reactions during acoustic cavitation. There is no CN^* in the solution, so that the excited-state CN radicals may come from the chemical reaction between CO_2, N_2, and water vapor in the air of the bubble. The subsequent spectroscopic signal of excited state Na^* implies gradual sonolytic introduction of Na contaminants originating from the glassware components and get excited in the plasma micro environments of the cavitation bubbles.

Only the Na^* atom emission line in the 360 nm–630 nm appears after the CN emission totally disappears. The Ar atom emission lines are visible when the spectral range is increased to 200 nm–900 nm. An uncalibrated spectrogram that shows Ar (4p–4s) atom emission lines in the red and near-infrared spectral lines as shown in Fig. 6. These lines are consistent with previous observations made in many experiments.[17,24] The resolvable atom emission lines have enabled interro-

gation of the bubble-liquid interfacial temperatures during collapse.[17]

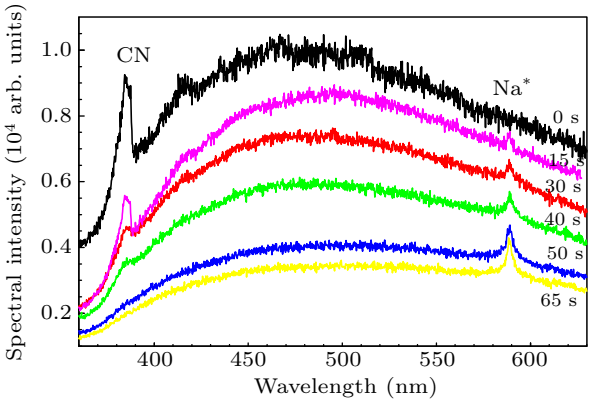


Fig. 5. The SL spectrum of dancing bubbles in the phosphoric acid solution obtained within the first few minutes of ultrasonic treatment. The indicated time represents the start of the corresponding measurement.

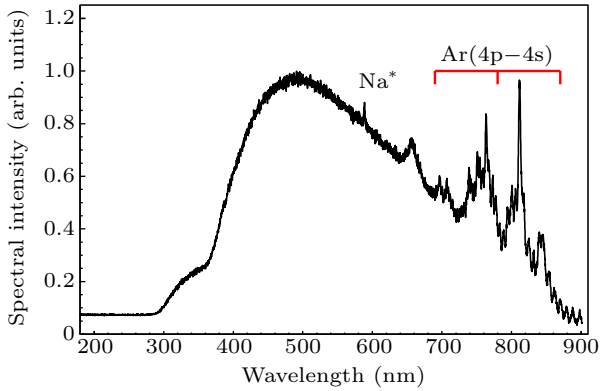


Fig. 6. The uncalibrated spectrum of MBSL in phosphoric acid saturated with Ar.

Comparable spectral transitions have been explained in many SL systems. The CN emission first appeared and then disappeared in a moving-SBSL investigation in adiponitrile solutions when the applied acoustic pressure was increased from 1.7 bar to 1.9 bar (1 bar = 10^5 Pa).[13] Despite increased brightness, a similar pressure-dependent disappearance of CN emission was reported for Ar-saturated SBSL in purified water at 25 °C.[19] The physical evolution of molecular band shapes signifies alterations in plasma properties, heating mechanisms, and chemical surroundings across discrete acoustical driving regimes. Additional exploration of such spectral transitions for cavitating bubbles in phosphoric acid could clarify whether distinct processes prevail in engendering electronically excited-state CN radicals and Na^* atom emission line under similar conditions.

3. Theoretical model

3.1. The bubble movement model

The numerical calculation model of bubble motion under the ultrasonic horn has been applied in some contributions.[27,31,32] The model is coupled to the translational dynamics based on the KM model of the single bubble.[23,33] The model mainly has the following form:

$$\left(1-\frac{\dot{R}}{c}\right)R\ddot{R}+\frac{3}{2}\left(1-\frac{\dot{R}}{3c}\right)\dot{R}^2=\frac{1}{\rho}\left(1+\frac{\dot{R}}{c}\right)p_{\rm s}+\frac{R}{\rho c}\frac{\mathrm{d}}{\mathrm{d}t}p_{\rm s}, \quad (1)$$

$$m\ddot{z}+\frac{2\pi}{3}\rho_0\frac{\mathrm{d}}{\mathrm{d}t}(R^3\boldsymbol{u})=-\frac{4\pi}{3}R^3\frac{\partial}{\partial z}P_{\rm ex}(z,t)+F_{\rm drag}, \quad (2)$$

where R is the bubble radius, c is sound speed in the surrounding liquid, $p_{\rm s}$ is the pressure at the bubble wall, the overdot denotes the time derivative. In the translational equation, $m=(4/3)\pi R_0^3\rho_{\rm g}$ is the gas mass of the bubble, $z(t)$ denotes the position of the bubble that is vertically located on the central axis of symmetry of the geometry under the ultrasonic horn, ρ_0 is the equilibrium density of phosphoric acid solution, and $\rho_{\rm g}$ is the equilibrium density of gas in bubble, $\boldsymbol{u}$ is the translational velocity of the bubble relative to the surrounding liquid, $P_{\rm ex}(z,t)$ is the acoustic driving pressure, $F_{\rm drag}$ is the viscous drag force on the bubble. The pressure at the bubble wall $p_{\rm s}$ is given by

$$p_{\rm s}=\frac{\rho}{4}\boldsymbol{u}\boldsymbol{u}+\left[P_{\rm g}-\frac{2\sigma}{R}-\frac{4\mu\dot{R}}{R}-p_{\rm ex}(z,t)-P_0+P_{\rm v}\right], \quad (3)$$

where $\boldsymbol{u}=\dot{z}(t)-v_{\rm ex}(z,t)$, where $\dot{z}(t)$ is the absolute translational velocity relative to the ultrasonic horn tip, $v_{\rm ex}(z,t)$ is the velocity of the surrounding liquid. σ is the surface tension, μ is the liquid viscosity, P_0 is hydrostatic pressure, $P_{\rm v}$ is vapor pressure, $P_{\rm g}$ is the internal gas pressure in the bubble

$$P_{\rm g}=\left(P_0+\frac{2\sigma}{R_0}\right)\left(\frac{R_0^3-h^3}{R^3-h^3}\right)^{\gamma}, \quad (4)$$

where h is the radius of van der Waals hard core ($h=R_0/8.86$) for Ar. And γ, the polytropic exponent, is a transition function from the isothermal behavior to the adiabatic behavior of the bubble interior. $\gamma(Pe)=1+(\Gamma-1)\exp(-A/Pe^B)$, is the adiabatic exponent for Ar and the parameters $A=5.8$ and $B=0.6$.[14] Obviously, $\gamma(Pe\to 0)\to 1$ isothermal behavior, where thermal diffusion is dominant and $\gamma(Pe\to\infty)\to 5/3$ adiabatic behavior, where advection is dominant, as it is required. The Peclet number Pe with the time dependeng, $Pe=|\dot{R}|R/\chi_{\rm Ar}$, where $\chi_{\rm Ar}$ is the thermal diffusivity of the gas

$$\chi_{\rm Ar}=(25/48)\Gamma^{-1}(\pi a_{\rm Ar}^2R_{\rm g}T/\mu_{\rm Ar})^{1/2}G(g) \quad (5)$$

with the molecular weight of Ar $\mu_{\rm Ar}=0.040$ kg/mol, the effective atomic diameter $a_{\rm Ar}=0.34$ nm, and the ideal gas constant $R_{\rm g}=8.31$, T is the gas temperature. Here $G(g)$ is a function of the dimensionless density, $g=2\pi N_a a_{\rm Ar}^2R_0^3/(3v_{\rm m}R^3)$, with the Avogadro's number $N_a=6.02\times10^{23}$ mol^{-1} and the specific molar volume $v_{\rm m}=0.022$ L/mol under normal conditions. The virial expansion approximation used in Enskog theory yields

$$G(g)=\frac{1}{g}\left(\frac{1}{\xi}+1.2g+0.755g^2\xi\right) \quad (6)$$

with $\xi = 1 + c_1 g + c_2 g^2 + c_3 g^3$, the virial coefficients $c_1 = 0.625$, $c_2 = 0.2869$, $c_3 = 0.115$.[14]

In the translational equation, $P_{\rm ex}(x,t)$ and $v_{\rm ex}(z,t)$ display in formula respectively as

$$P_{\rm ex}(z,t) = {\rm Re}\left\{\hat{v}\rho c\left({\rm e}^{-{\rm i}kz} - {\rm e}^{-{\rm i}k\sqrt{z^2+a^2}}\right){\rm e}^{{\rm i}2\pi ft}\right\}, \quad (7)$$

$$v_{\rm ex}(z,t) = {\rm Re}\left\{\hat{v}\left({\rm e}^{-{\rm i}kz} - \frac{z{\rm e}^{{\rm i}k\sqrt{z^2+a^2}}}{\sqrt{z^2+a^2}}\right){\rm e}^{{\rm i}2\pi ft}\right\}, \quad (8)$$

with the velocity amplitude $\hat{v}$, the radius of horn tip a, and the wave number vector of an ultrasonic wave k. The viscous drag force $F_{\rm drag}$ on the bubble can be expressed as

$$F_{\rm drag} = -\frac{\pi}{2} C_{\rm D} \rho_0 R^2 |\boldsymbol{u}| \boldsymbol{u}, \quad (9)$$

with a suitable drag coefficient $C_{\rm D}$ that matches the asymptotic limits of high and low Reynolds numbers $Re = 2R|\boldsymbol{u}|\rho/\mu$:

$$C_{\rm D} = \frac{16}{Re}\left\{1 + \left[\frac{8}{Re} + \frac{1}{2}\left(1 + 3.315 Re^{-1/2}\right)\right]^{-1}\right\}. \quad (10)$$

The system of Eqs. (1)–(10) constitutes a closed ODE system for R, $\dot{R}$, z, and $\dot{z}$. In the simulations, the following general parameters for 85-wt% phosphoric acid solution and Ar at room temperature were used: $\sigma = 0.136$ N/m, $\rho = 1691.4$ kg/m^3, $c = 1650$ m/s, $\mu = 47$ mPa·S, $P_0 = 1.013 \times 10^5$ Pa, $\rho_{\rm g} = 1.7837$ kg/m^3, $f = 20$ kHz, $\hat{v} = 0.4$ m/s.

3.2. The bubble temperature model

Since we can observe bright light and strong CN ($B^2\Sigma$–$X^2\Sigma$) emission from MBSL in phosphoric acid solution, and a fine structure of Ar (4p–4s) transitions, this can be used as a spectroscopic probe to quantify the temperature within the bubble in solution.[19] The effective emission temperature of CN ($B^2\Sigma$–$X^2\Sigma$) can be obtained by fitting the experimental spectrum to simulated emission spectrum from the LIFBASE program. LIFBASE is a database and spectral simulation program designed for diatomic molecules, extensively used for temperature determination of diatomic molecules through excitation in flame and laser-induced fluorescence.[23,27,33] Similarly, the plasma temperature preserved during bubble collapse was approximated by modeling the Ar (4p–4s) atom emission lines and neighboring continuum emission.[22]

The intensity of an atom emission line corresponding to radiative relaxation (both induced and spontaneous processes) from an electronically excited-state can be expressed as

$$I_{nm} = \frac{hc}{\lambda_{nm}} A_{nm} g_n \frac{1}{4\pi Q(T)} \exp\left(\frac{-E_n}{kT}\right) l\rho_0. \quad (11)$$

Here, h is Planck's constant, c is the speed of light, k is the Boltzmann constant, λ_{nm} represents the transition wavelength, g_n is the degeneracy of the excited upper state, $Q(T)$ gives the temperature-dependent partition function $\sum_n g_n \exp(-E_n/kT)$, A_{nm} is the Einstein transition probability between states n and m, E_n is the energy of the upper state n, l is the path length of the confining region, ρ_0 refers to the absorber atom density, and kT represents the absolute temperature.

In principle, we can compare the calculated calibration curves (i.e., I_{nm} versus T) with experimental spectroscopic measurements of the absolute line intensities of specific leaps to determine the temperature at which the bubble occurs at the time of collapse.

When the system under study conforms to the Maxwell–Boltzmann distribution, the two-line radiance ratio method is simpler because it does not require knowledge of the path lengths and atomic number densities, only the relative Einstein transition probabilities.[23] The method determines the gas temperature by measuring the relative totality of two or more states and determining the temperature that best fits the data.

The ratio of the intensities of the two emission lines can be derived from Eq. (11) and expressed as

$$\frac{I_1}{I_2} = \frac{g_1 A_1 \lambda_1}{g_2 A_2 \lambda_2} \cdot l \cdot \exp(E_2 - E_1)/kT, \quad (12)$$

where the subscripts refer to the two spectral lines being compared. When the g, A, λ, and E of an Ar atom are fairly accurate, then the absolute temperature can be determined by measuring the relative intensities of the two emission lines produced by the leaps from different excited states. It is important to integrate the light intensity throughout the frequency while taking spectral line broadening into account. When a cavitation bubble is emitting light, the atoms are very closely spaced, as in a solid, the bubble radius is reduced, and the wave functions overlap, broadening the spectral lines. By adjusting the variance at different temperatures, the atom emission lines can be fitted to form Gaussian distributed peaks. The values used in the computations are derived from Ref. [35].

4. Result and discussion

4.1. Bubble motion at different initial positions

The bubble motion equations were used to simulate the motion of the dancing bubbles with different initial positions under the ultrasonic horn, as shown in Fig. 7. It can be seen that most of the dancing bubbles move upward from below the ultrasonic horn so that the observed motion roughly matches the estimated motion of the bubbles in space. In this instance, it moves back and forth regularly over a small area, essentially stagnating. However, a closer examination shows that

occasionally the model predicts a net downward translation, while the motion of the bubble would translate upward (as shown in Fig. 4(b), near the ultrasonic horn). This indicates that the piston field hypothesis does not accurately reproduce the pressure field, especially the phase between the acoustic intensity and its gradient. As the presented model assumes two-dimensional bubble motion, more complex three-dimensional dynamics observed experimentally may not be perfectly reproduced computationally.

The motion of these bubbles is consistent with spherical bubbles in sulfuric acid solutions. Andrea *et al.* showed that the dynamics of MBSL and the resulting temperature field can be very complex.[27,36] The morphology of MBSL at different acoustic pressures is similarly complex and variable. Our observations of filamentary structures and dancing bubbles confirm these findings, especially the transition from filamentary to clustered bubbles with increasing acoustic power.

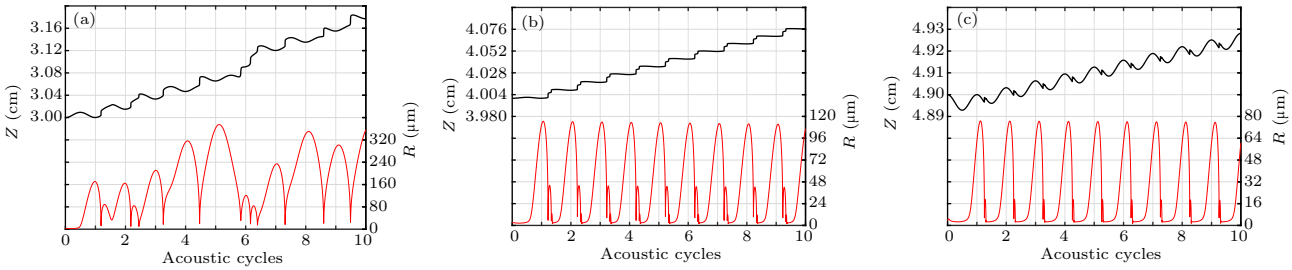


Fig. 7. The red solid line represents the radius variation curve of dancing bubbles at different positions, while the black solid line represents the position variation of bubbles with acoustic cycles: (a) $z = 3$ cm, (b) $z = 4$ cm, (c) $z = 4.9$ cm.

4.2. Internal temperature of dancing bubbles

The spectral code LIFBASE was used to simulate the emission from the CN ($B^2\Sigma$–$X^2\Sigma$) emission after normalization and baseline subtraction. In order to best fit the experimental spectrum, the input parameters for vibrational temperature T, rotational temperature T_r, and effective pressure p were manually adjusted. The light intensity is still weak at the beginning of the SL phenomena in the phosphoric acid solution, and the temperature inside the bubble can be approximately 8900 K at this time based on the CN emission in Fig. 8(a). In addition, there is a significant C_2 emission in the wavelength between 450 nm and 600 nm. The Na^* atom emission line gets more visible with the increase of ultrasonic irradiation time, while the CN emission and C_2 emission finally disappear. At the same time, the Ar atom emission lines becomes stronger. One clear indicator that plasma nuclei were present during bubble collapse is the production of Ar atom emission lines. Using the two-line radiance ratio method, the Ar atom emission lines were also fitted after normalization and the baseline subtraction. Figure 8(b) shows that the temperature within the dancing bubble, as determined by the two-line radiance ratio method is around 14000 K.

The progressive enhancement of plasma temperatures under constant ultrasonic driving implies gradual intensification of bubble collapse in the degassing phosphoric acid solutions. The initial emergence of electronically excited-state CN radicals signifies the presence of dissolved atmospheric components, with potential formation mechanisms including:

$$CO_2 + N_2 \rightarrow CN + NO_2. \tag{13}$$

We found that at the begining of experiment the SL intensity increased with the irradiation time, as the solution temperature rose, the solubility dropped, CO_2 and N_2 gases escaped, enriching the solution with Ar. However, beyond a certain irradiation time, the SL intensity decreased, as the solution temperature exceeded the optimal range for Ar bubble formation and the solution viscosity altered.

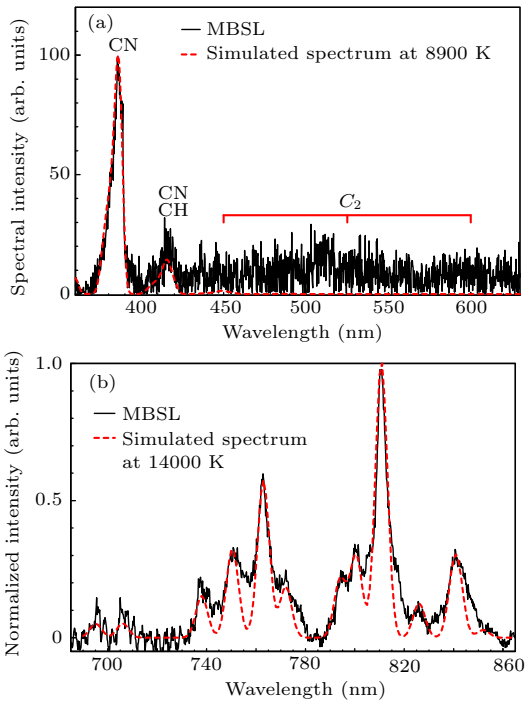


Fig. 8. (a) The spectrum at the beginning of the dancing bubble SL and the results of fitting using the LIFBASE code. (b) The Ar atom emission lines from dancing bubble SL in the phosphoric acid solution compared to a calculated Ar atom emission spectrum at 14000 K.

Experimental results indicate significant temperature variations within the MBSL. Similar observations were re-

ported by Xu *et al*., who identified spatial separation of sonoluminescing bubbles in sulfuric acid solutions.[23] Their findings suggest that different regions within the bubble cloud experience varying thermal conditions, which qualitatively align with our data. Furthermore, Suslick *et al*. reported effective emission temperatures approaching 20000 K within collapsing bubbles,[24] supporting the high-temperature conditions inferred in our experiments.

5. Conclusion

The dancing bubble SL were studied in an 85-wt% phosphoric acid solution containing saturated Ar. The paths traversed by the dancing bubble SL during the camera exposure period were observed to exhibit an irregular dynamic motion, crossing paths that fell within the general range of a 25-mm^2 area. Through rigorous spectral analyses spanning a wavelength range of 200 nm to 900 nm, the study reveals Ar atom emission lines and phenomena originating from CN ($B^2\Sigma$–$X^2\Sigma$) emission.

We have studied dancing bubbles in terms of motion equations and temperature modeling. Most of the dancing bubble observed in the experiments showed a pattern of motion consistent with the simulations, but certain specific states of motion proved to be difficult to simulate, suggesting potential limitations of the theoretical model. Comparative evaluation of temperature models and spectra reveals a phenomenon characterized by a gradual increase and then decrease in temperature within the SL bubbles when the experiment is first performed. This experiment is of great academic significance for advancing our understanding of the SL principles and the complex dynamics of dancing bubble SL.

Acknowledgements

Project supported by the Scientific Research Project of Higher Education in the Inner Mongolia Autonomous Region, China (Grant No. NJZY23100) and the Natural Science Foundation of Inner Mongolia Autonomous Region, China (Grant No. 2024FX30), and the 14th Five Year Plan Project for Education Science in Inner Mongolia Autonomous Region, China (Grant No. NGJGH2023205).

References

[1] Gaitan D F, Crum L A, Church C C and Roy R 1992 *J. Acoust. Soc. Am.* **91** 3166
[2] Walton A J and Reynolds G T 1984 *Adv. Phys.* **33** 595
[3] Marinesco N and Trillat J J 1933 *C. R. Acad. Sci.* **196** 858
[4] Frenzel H and Schultes H 1934 *Z. Phys. Chem.* **27** 421
[5] Taylor K J and Jarman P D 1970 *Aust. J. Phys* **23** 319
[6] Didenko Y T and Suslick K S 2000 *Phys. Rev. Lett.* **84** 777
[7] Chakravarty A, Georghiou T, Phillipson T E and Walton A J 2004 *Phys. Rev. E* **69** 066317
[8] Flannigan D J and Suslick K S 2005 *Nature* **434** 52
[9] Chen W Z, Huang W, Liang Y, Gao X X and Cui W C 2008 *Phys. Rev. E* **78** 035301
[10] An Y and Li C 2009 *Phys. Rev. E* **80** 046320
[11] Hopkins S D, Putterman S J, Kappus B A, Suslick K S and Camara C G 2005 *Phys. Rev. Lett.* **95** 254301
[12] Toegel R, Gompf B, Pecha R and Detlef L 2000 *Phys. Rev. Lett.* **85** 3165
[13] Didenko Y T, Rd M N W and Suslick K S 2000 *Nature* **407** 877
[14] Hilgenfeldt S, Grossmann S and Lohse D 1999b *Phys. Fluids* **11** 1318
[15] Holzfuss J, Ruggeberg M and Mettin R 1998 *Physics* **81** 1961
[16] Hiller R, Weninger K, Putterman S and Barber B P 1994 *Science* **266** 248
[17] Eddingsaas N C and Suslick K S 2007 *J. Am. Chem. Soc.* **129** 3838
[18] Xu J F, Chen W Z and Liang Y 2007 *Chin. Sci. Bull.* **52** 1237
[19] Flynn H G 1964 *Physical Acoustics* (New York: W. P. Mason) p. 57
[20] Troia A, Madonna D and Spagnolo R 2006 *Ultrason. Sonochem.* **13** 287
[21] David J F and Suslick K 2007 *Phys. Rev. Lett.* **99** 134301
[22] Xu H X, Glumac N G and Suslick K S 2010 *Angew. Chem. Int. Ed.* **49** 1079
[23] Xu H X, Eddingsaas N C and Suslick K S 2009 *J. Am. Chem. Soc.* **131** 6060
[24] Suslick K S and Flannigan D J 2008 *Annu. Rev. Phys. Chem.* **59** 659
[25] Sadighibonabi R, Mirheydari M, Rezaee N and Ebrahimi H 2011 *Phys. Rev. E* **84** 026301
[26] Rossell J M, Dellavale D and Bonetto F J 2015 *Ultrason. Sonochem.* **22** 59
[27] Thiemann A, Frank H, Carlos C and Mettin R 2017 *Ultrason. Sonochem.* **34** 663
[28] Dellavale D, Rechiman L, Rossello J and Bonetto F 2012 *Phys. Rev. E* **86** 016320
[29] Sadighibonabi R, Rezaee N and Galavan Z 2009 *J. Acoust. Soc. Am.* **126** 2266
[30] Sadighibonabi R, Mirheydari M, Ebrahimi H, Rezaee N and Nikzad L 2011 *Chin. Phys. B* **20** 252
[31] Liang J F, Xiong D F, An Y and Chen W Z 2022 *Chin. Phys. B* **31** 117802
[32] Al Bishtawi B, Mustapha K B and Scribano G 2024 *Phys. Fluids* **36** 043336
[33] Fabian D and Schenke S 2023 *Phys. Fluids* **35** 012114
[34] Xu X Y, Jiang J K, Chen W Q, *et al*. 2022 *Chin. Phys. B* **31** 068503
[35] Kramida A, Ralchenko Yu, Reade J, and NIST ASD Team. *NIST Atomic Spectra Database* (ver. 5.11) National Institute of Standards and Technology, Gaithersburg, MD. https://physics.nist.gov/PhysRefData/ASD/lines-form.html
[36] Shen Y, Zhang L, Wu Y, *et al*. 2021 *Ultrason. Sonochem.* **73** 105535